Inorg. Chem. **2008**, *47*, 101–112

Zinc Carboxylate Cluster Formation in Conjugated Metallomacrocycles: Evidence for Templation

Peter D. Frischmann, Amanda J. Gallant, Jonathan H. Chong, and Mark J. MacLachlan*

Department of Chemistry, University of British Columbia, 2036 Main Mall, Vancouver, British Columbia V6T 1Z1, Canada

Received July 11, 2007

A new [3 + 3] Schiff base macrocycle incorporating three N_2O_2 salphen-type binding sites and peripheral neopentyloxy substituents has been prepared. The incorporation of Zn^{2+} ions into this and related conjugated Schiff base macrocycles has been studied by NMR spectroscopy, mass spectrometry, and X-ray diffraction. When reacted with 7 equiv of zinc acetate, the macrocycles template the formation of heptanuclear complexes. Two tetranuclear Zn^{2+} complexes that are plausible intermediates in the assembly of the heptanuclear complexes have been isolated and structurally characterized. These reactive intermediates are promising substrates for the synthesis of polynuclear, mixed-metal clusters. We also demonstrate that this chemistry may be generalized to other bridging carboxylate ligands, such as methacrylate.

Introduction

Unusual optical and magnetic properties frequently arise when metal ions are confined to well-defined molecular clusters, making these multimetallic clusters attractive building blocks for functional materials.[1] These complexes are also often of interest as models for the active sites of enzymes, such as the FeMo cluster in nitrogenase. Controlling the nuclearity of cluster complexes presents a challenge that may be solved using supramolecular chemistry. Macrocyclic ligands with several donor atoms often coordinate polynuclear transition-metal complexes in their interior and may serve as a scaffold for the synthesis of molecular metal clusters. Polynuclear complexes have been reported inside Robson-type macrocycles,[2] sulfonylcalixarenes,[3] thiacalixarenes,[4] and a variety of other organic macrocycles. Recently, a tetradecanuclear copper(II) cluster templated inside two multidentate macrocycles was reported by Tandon et al.[5] In general, metal clusters may be coordinated within the preformed macrocycle or, as is often the case, they may template the formation of the macrocycle.

Metal cluster formation inside macrocycles is not well understood. These complexes are usually obtained by hydrothermal methods and it is assumed that the thermodynamic product is obtained, but little thought is given to the mechanism of cluster formation. The synthesis of complex multimetallic cluster complexes, such as the FeMo cluster found in nitrogenase, will undoubtedly require a templating mechanism in which metal atoms are incorporated in a stepwise fashion. Mechanistic insight into metal cluster formation will aid in the development of new clusters and enhance researchers' synthetic control over existing multimetallic clusters.

We and others have been investigating the chemistry of Schiff base macrocycles.[6,7] In particular, the macrocycles of interest to us are shape-persistent, conjugated Schiff base

* To whom correspondence should be addressed. E-mail: mmaclach@chem.ubc.ca.

(1) (a) Kong, X.-J.; Ren, Y.-P.; Long, L.-S.; Zheng, Z.; Huang, R.-B.; Zhen, L.-S. *J. Am. Chem. Soc.* **2007**, *129*, 7016−7017. (b) Bolink, H. J.; Cappelli, L.; Coronado, E.; Recalde, I. *Adv. Mater.* **2006**, *18*, 920−923. (c) Ako, A. M.; Hewitt, I. J.; Mereacre, V.; Clérac, R.; Wernsdorfer, W.; Anson, C. E.; Powell, A. K. *Angew. Chem., Int. Ed.* **2006**, *45*, 4926−4929. (d) Hou, H.; Wei, Y.; Song, Y.; Mi, L.; Tang, M.; Li, L.; Fan, Y. *Angew. Chem., Int. Ed.* **2005**, *44*, 6067−6074. (e) Jian, F.; Xiao, H.; Bai, Z.; Zhao, P. *J. Mater. Chem.* **2006**, *16*, 3746−3752.

(2) (a) Tandon, S. S.; Thompson, L. K.; Bridson, J. N. *J. Chem. Soc., Chem. Commun.* **1992**, 911−913. (b) Tandon, S. S.; Thompson, L. K.; Bridson, J. N.; Benelli, C. *Inorg. Chem.* **1995**, *34*, 5507−5515. (c) Bell, M.; Edwards, A. J.; Hoskins, B. F.; Kachab, E. H.; Robson, R. *J. Am. Chem. Soc.* **1989**, *111*, 3603−3610.

(3) (a) Kajiwara, T.; Katagiri, K.; Hasegawa, M.; Ishii, A.; Ferbinteanu, M.; Takaishi, S.; Ito, T.; Yamashita, M.; Iki, N. *Inorg. Chem.* **2006**, *45*, 4880−4882. (b) Kajiwara, T.; Kobashi, T.; Shinagawa, R.; Ito, T.; Takaishi, S.; Yamashita, M.; Iki, N. *Eur. J. Inorg. Chem.* **2006**, 1765−1770.

(4) Kajiwara, T.; Kon, N.; Yokozawa, S.; Ito, T.; Iki, N.; Miyano, S. *J. Am. Chem. Soc.* **2002**, *124*, 11274−11275.

(5) Tandon, S. S.; Bunge, S. D.; Thompson, L. K. *Chem. Commun.* **2007**, 798−800.

(6) Vigato, P. A.; Tamburini, S.; Bertolo, L. *Coord. Chem. Rev.* **2007**, *251*, 1311−1492.

10.1021/ic701385m CCC: $40.75
Published on Web 12/08/2007

Scheme 1. Reaction of Shape-Persistent, Conjugated Schiff Base Macrocycles **1a**−**d** with Zinc Acetate Yields Heptazinc Cluster Complexes **7a**−**d**[a]

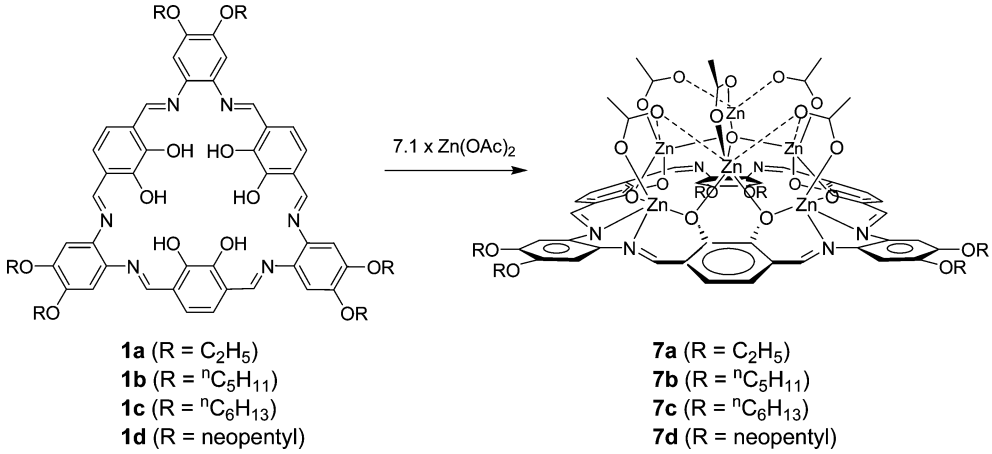

1a (R = C_2H_5)
1b (R = $^nC_5H_{11}$)
1c (R = $^nC_6H_{13}$)
1d (R = neopentyl)

7a (R = C_2H_5)
7b (R = $^nC_5H_{11}$)
7c (R = $^nC_6H_{13}$)
7d (R = neopentyl)

[a]The seventh zinc ion and sixth acetate ligand are obscured by the depiction of the cluster.

macrocycles such as **1a**−**d**, which possess three N_2O_2 coordination sites for metal complexation (Scheme 1).[8,9] Moreover, these rings have a crown-ether-like interior composed of six hydroxyl groups with the potential to further coordinate metals. We have demonstrated that the metal-free, Schiff base macrocycles coordinate alkali metals in the central hexa(hydroxy) interior rather than in the N_2O_2 pockets.[10] Recently, Nabeshima et al. coordinated a lanthanum ion in this same environment to template a related oxime-based macrocycle.[11]

We recently communicated that macrocycles **1a**−**c** can coordinate $[Zn_4O]^{6+}$ clusters in their interiors.[12] Macrocyclic complexes of zinc are attractive as models for the active sites of metalloenzymes such as alkaline phosphatase, P1 nuclease, and phospholipase C, the latter two both possessing trinuclear zinc clusters in the active site.[13] Zacharias and co-workers reported DNA cleavage by a trinuclear zinc complex formed within a chiral macrocycle.[14] The same complex was used by Gao et al. to catalyze asymmetric aldol and Henry reactions.[15] Other catalytic reactions, including carboxy- and phosphate-ester hydrolysis and the direct catalytic conversion of lactones and esters to oxazolines have been demonstrated using high-nuclearity zinc complexes.[16]

Reactions involving a zinc source and a carboxylate ligand most often yield three-dimensional networks or layered structures, but occasionally, multinuclear molecular cluster compounds are isolated. The most common molecular zinc carboxylate cluster, basic zinc acetate, consists of a tetrahedral $[Zn_4(\mu_4\text{-O})]^{6+}$ core with six acetate ligands bridging the zinc ions in a μ-1,2 fashion.[17] Tetranuclear cubane,[18] drumlike hexanuclear dicubane,[19] as well as double tetrahedral heptanuclear zinc clusters have also been synthesized.[20] Roesky et al. reacted *tert*-butylphosphonic acid in THF with $ZnEt_2$ in toluene, resulting in the highest nuclearity molecular zinc oxo complex to date, a dodecanuclear zincophosphate aggregate that consists of a $[Zn_4(\mu_4\text{-O})]^{6+}$ core and a zincophosphonate shell.[21] In general, the clusters of zinc complexes that have been obtained are by chance and are usually not stable in solution.

In this Article, we report our investigations of the incorporation of zinc into the Schiff base macrocycles **1a**−**d**,

(7) For recent examples of multinuclear complexes in Schiff base macrocycles, see: (a) Volpe, M.; Reid, S. D.; Blake, A. J.; Wilson, C.; Love, J. B. *Inorg. Chim. Acta* **2007**, *360*, 273−280. (b) Wang, J.; Slater, B.; Alberola, A.; Stoeckli-Evans, H.; Razavi, F. S.; Pilkington, M. *Inorg. Chem.* **2007**, *46*, 4763−4765. (c) de Geest, D. J.; Noble, A.; Moubaraki, B.; Murray, K. S.; Larsen, D. S.; Brooker, S. *Dalton Trans.* **2007**, 467−475. (d) Sessler, J. L.; Tomat, E.; Lynch, V. M. *J. Am. Chem. Soc.* **2006**, *128*, 4184−4185. (e) Hui, J. K.-H.; MacLachlan, M. J. *Chem. Commun.* **2006**, 2480−2482.

(8) MacLachlan, M. J. *Pure Appl. Chem.* **2006**, *78*, 873−888.

(9) (a) Huck, W. T. S.; van Veggel, F. C. J. M.; Reinhoudt, D. N. *Recl. Trav. Chim. Pays-Bas* **1995**, *114*, 273−276. (b) Akine, S.; Taniguchi, T.; Nabeshima, T. *Tetrahedron Lett.* **2001**, *42*, 8861−8864. (c) Gallant, A. J.; Hui, J. K.-H.; Zahariev, F. E.; Wang, Y. A.; MacLachlan, M. J. *J. Org. Chem.* **2005**, *70*, 7936−7946. (d) Ma, C.; Lo, A.; Abdolmaleki, A.; MacLachlan, M. J. *Org. Lett.* **2004**, *6*, 3841−3844. (e) Ma, C. T.-Z.; MacLachlan, M. J. *Angew. Chem., Int. Ed.* **2005**, *44*, 4173−4182. (f) Gallant, A. J.; Sauer, M.; Yun, M.; Yeung, C. S.; MacLachlan, M. J. *Org. Lett.* **2005**, *7*, 4827−4830. (g) Nabeshima, T.; Miyazaki, H.; Iwasaki, A.; Akine, S.; Saiki, T.; Ikeda, C. *Tetrahedron* **2007**, *63*, 3328−3333. (h) Frischmann, P. D.; MacLachlan, M. J. *Chem. Commun.* **2007**, 4480−4482..

(10) Gallant, A. J.; MacLachlan, M. J. *Angew. Chem., Int. Ed.* **2003**, *42*, 5307−5310.

(11) Akine, S.; Sunaga, S.; Taniguchi, T.; Miyazaki, H.; Nabeshima, T. *Inorg. Chem.* **2007**, *46*, 2959−2961.

(12) (a) Gallant, A. J.; Chong, J. H.; MacLachlan, M. J. *Inorg. Chem.* **2006**, *45*, 5248−5250. (b) Nabeshima, T.; Miyazaki, H.; Iwasaki, A.; Akine, S.; Saiki, T.; Ikeda, C.; Sato, S. *Chem. Lett.* **2006**, *35*, 1070−1071.

(13) Parkin, G. *Chem. Rev.* **2004**, *104*, 699−767.

(14) Korupoju, S. R.; Mangayarkarasi, N.; Zacharias, P. S.; Mizuthani, J.; Nishihara, H. *Inorg. Chem.* **2002**, *41*, 4099−4101.

(15) Gao, J.; Zingaro, R. A.; Reibenspies, J. H.; Martell, A. E. *Org. Lett.* **2004**, *6*, 2453−2455.

(16) (a) Bazzicalupi, C.; Bencini, A.; Berni, E.; Giorgi, C.; Maoggi, S.; Valtancoli, B. *Dalton Trans.* **2003**, 3574−3580. (b) Ohshima, T.; Iwasaki, T.; Mashima, K. *Chem. Commun.* **2006**, 2711−2713.

(17) Koyama, H.; Saito, Y. *Bull. Chem. Soc. Jpn.* **1954**, *27*, 112−114.

(18) (a) Driess, M.; Merz, K.; Schoenen, R. *Organometallics* **2007**, *26*, 2133−2136. (b) Murugavel, R.; Kuppuswamy, S.; Boomishankar, R.; Steiner, A. *Angew. Chem., Int. Ed.* **2006**, *45*, 5536−5540. (c) Hudson, T. A.; Berry, K. J.; Moubaraki, B.; Murray, K. S.; Robson, R. *Inorg. Chem.* **2006**, *45*, 3549−3556. (d) Polarz, S.; Orlov, A. V.; van den Berg, M. W. E.; Driess, M. *Angew. Chem., Int. Ed.* **2005**, *44*, 7892−7896.

(19) Westerhausen, M.; Sapelza, G.; Gŏrls, H.; Mayer, P. *Inorg. Chem.* **2006**, *45*, 409−414.

(20) (a) Lalioti, N.; Raptopoulou, C. P.; Terzis, A.; Aliev, A. E.; Perlepes, S. P.; Gerothanassis, I. P.; Manessi-Zoupa, E. *Chem. Commun.* **1998**, 1513−1514. (b) Waheed, A.; Jones, R. A.; McCarty, J.; Yang, X. *Dalton Trans.* **2004**, 3840−3841.

(21) Yang, Y.; Pinkas, J.; Noltemeyer, M.; Schmidt, H.-G.; Roesky, H. W. *Angew. Chem., Int. Ed.* **1999**, *38*, 664−666.

affording heptanuclear complexes **7a**−**d** as illustrated in Scheme 1. The isolation and characterization of two intermediate tetranuclear complexes strongly suggests that macrocycles **1a**−**d** template the formation of $[Zn_4O]^{6+}$ clusters and provides insight into the mechanism of metal cluster assembly. These tetranuclear complexes exhibit unusual metal-ion ring walking behavior and may function as scaffolds for the templation of mixed-metal cluster complexes. Macrocycles **1a**−**d** are promising hosts for the development of well-defined mixed-metal clusters.

Experimental Section

Zinc(II) acetate dihydrate and zinc(II) methacrylate were obtained from Aldrich. Compounds **1a**−**c**,[9c] **2**,[22] **5**,[9b] and **7a**−**c**[12a] were prepared according to literature procedures.

Synthesis of 1,2-Dineopentyloxy-4,5-dinitrobenzene (3). 1,2-Dineopentyloxybenzene **2**[22] (4.0 g, 16.0 mmol) was added to 50 mL of concentrated nitric acid and heated to 60 °C. A yellow precipitate formed after 30 min, and after 12 h, the reaction mixture was poured into 400 mL of water. The yellow solid was isolated on a Buchner funnel, washed with water, and recrystallized from hot EtOH, affording large yellow needles. Yield: 3.2 g (9.4 mmol, 59%).

Data for 3. ^{13}C NMR (100.6 MHz, $CDCl_3$): δ 152.3, 136.6, 107.5, 79.5, 32.3, 26.6. ^{1}H NMR (400 MHz, $CDCl_3$): δ 7.24 (s, 2H, Ar), 3.72 (s, 4H, OCH_2), 1.10 (s, 18H, CH_3). UV−vis (CH_2Cl_2) λ_{max} (ϵ) = 343 (3.03×10^5), 274 (1.41×10^5), 247 (1.15×10^5) nm (L mol^{-1} cm^{-1}). EI-MS: m/z = 340 (**3**)$^+$, 255 (**3** − $OCH_2C(CH_3)_3$)$^+$. IR (KBr) υ = 3432, 3071, 2971, 2959, 2872, 1586, 1530, 1478, 1378, 1366, 1336, 1292, 1266, 1228, 1045, 1014, 984, 941, 872, 818, 753, 637 cm^{-1}. Mp 168 °C. Anal. Calcd for **3**, $C_{16}H_{24}N_2O_6$: N, 8.23; C, 56.46; H, 7.11. Found: N, 8.60; C, 56.67; H, 6.95.

Synthesis of 4,5-Diamino-1,2-dineopentyloxybenzene (4). In a Schlenk flask, compound **3** (4.5 g, 13.2 mmol) was suspended in 100 mL of EtOH degassed with N_2. After 30 min, the flask was charged with 4 mL of hydrazine monohydrate and approximately 750 mg of Pd/C. The Schlenk flask was then fitted with a condenser and heated to 70 °C under N_2. Raney Ni was added after 12 h, and 4 h later the reaction was filtered through Celite using inert atmosphere techniques. The removal of solvent under vacuum gave compound **4**, an air-sensitive white powder. Yield: 3.376 g (12.0 mmol, 91%)

Data for 4. ^{13}C NMR (100.6 MHz, $CDCl_3$): δ 144.0, 128.3, 106.5, 80.7, 32.4, 26.9. ^{1}H NMR (300 MHz, $CDCl_3$): δ 6.37 (s, 2H, Ar), 3.55 (s, 4H, OCH_2), 3.17 (s, 4H, amine), 1.04 (s, 18H, CH_3). EI MS: m/z = 280 (**4**)$^+$, 210 (**4** − C_5H_{11})$^+$, 140 (**4** − $(C_5H_{11})_2$)$^+$.

Synthesis of Macrocycle 1d (R = $CH_2{}^t$Bu). A Schlenk flask was charged with **4** (2.0 g, 7.1 mmol) and dissolved in 30 mL of degassed 1:2 $CHCl_3$/MeCN. The addition of 1,4-diformyl-2,3-dihydroxybenzene **5**[9b] (1.19 g, 7.1 mmol) to the clear, light yellow solution resulted in a deep red color. The flask was fitted with a condenser, and the reaction mixture was heated to reflux (80 °C) for 2 h under an atmosphere of nitrogen. After cooling to room temperature, the dark red microcrystalline precipitate of **1d** was isolated on a Buchner funnel. Yield: 2.45 g (2.0 mmol, 84%). Macrocycle **1d** was recrystallized from hot *N*,*N*-dimethylformamide (DMF) for elemental analysis. The macrocycle was not sufficiently soluble to obtain a ^{13}C NMR spectrum.

Data for 1d (R = $CH_2{}^t$Bu). ^{1}H NMR (300 MHz, DMF-d_7): δ 13.80 (s, 6H, OH), 9.16 (s, 6H, imine), 7.42 (s, 6H, Ar), 7.20 (s, 6H, Ar), 3.88 (s, 12H, OCH_2), 1.13 (s, 54H, CH_3). UV−vis (CH_2Cl_2) λ_{max} (ϵ) = 343 (8.03×10^5), 406 (1.09×10^6) nm (L mol^{-1} cm^{-1}). MALDI-TOF: m/z = 1231 (**1d**)$^+$, 1253 (**1d** + Na)$^+$, 1268 (**1d** + K)$^+$, 2506 (**1d**$_2$ + Na)$^+$. IR (KBr): υ = 3440, 2955, 2904, 2869, 1612, 1514, 1495, 1476, 1456, 1301, 1259, 1221, 1190, 1009 cm^{-1}. Mp >270 °C. Anal. Calcd for **1d**, $C_{72}H_{90}N_6O_{12}$·DMF: N, 7.55; C, 69.37; H, 7.06. Found: N, 7.33; C, 69.06; H, 7.21.

Synthesis of the Heptazinc Complex 7d (R = $CH_2{}^t$Bu). Zinc acetate dihydrate (66 mg, 0.30 mmol) was added to a stirring suspension of **1d** (52 mg, 42.3 μmol) in 5 mL of ethanol. Upon the addition of zinc acetate, the deep red solution rapidly turned bright orange. After stirring at room temperature for 2 h, the reaction mixture was filtered and **7d** was isolated as an orange powder. Yield: 61 mg (30 μmol, 70%). Recrystallization from hot DMF afforded analytically pure **7d**. Single crystals suitable for X-ray diffraction were also obtained from DMF.

Data for 7d (R = $CH_2{}^t$Bu). ^{13}C NMR (100.6 MHz, DMF-d_7): δ 174.8, 158.9, 135.1, 122.2, 121.0, 103.0, 100.9, 79.6, 33.0 , 27.2, 24.1, 22.5. ^{1}H NMR (300 MHz, DMF-d_7): δ 8.85 (s, 6H, imine), 7.55 (s, 6H, Ar), 6.95 (s, 6H, Ar), 3.93 (d, J_{HH} = 8.8 Hz, 6H, OCH_2), 3.89 (d, J_{HH} = 8.8 Hz, 6H, OCH_2), 1.90 (s, 9H, OAc), 1.74 (s, 9H, OAc), 1.14 (s, 54H, $C(CH_3)_3$). UV−vis (CH_2Cl_2) λ_{max} (ϵ) = 242 (8.9×10^5), 348 (7.9×10^5), 419 (1.5×10^6) nm (L mol^{-1} cm^{-1}). MALDI-TOF: m/z = 1604.3 (**7d**−$Zn_3(OAc)_4$−O)$^+$, 1746.3 (**7d**−$Zn_2(OAc)_3$+H)$^+$, 1811.3 (**7d**−$Zn(OAc)_3$)$^+$, 1993.1 (**7d**−OAc)$^+$, 2054.1 (**7d**)$^+$. IR (KBr): υ = 3440, 2956, 2906, 2870, 1612, 1508, 1463, 1456, 1321, 1262, 1221, 1182, 1112, 1045, 1018, 568, 493 cm^{-1}. Mp >270 °C. Anal. Calcd for **7d**, $C_{84}H_{102}N_6O_{25}Zn_7$·2DMF: N, 5.09; C, 49.14; H, 5.32. Found: N, 5.31; C, 49.51; H, 5.39.

Synthesis of Tetrazinc Complex 8 (R = $CH_2{}^t$Bu). Complex **8** was prepared following the procedure for heptazinc complex **7d**, but the stoichiometry of **1d** to $Zn(OAc)_2$ was 1:4 (50 mg, 41 μmol of macrocycle **1d** and 35.6 mg, 0.16 mmol of zinc acetate dihydrate). Complex **8** was isolated as an orange powder by filtration and recrystallized from hot DMF. Yield: 40 mg (25 μmol, 61%). Low symmetry and poor solubility prevented analysis by ^{13}C NMR spectroscopy. Single crystals suitable for X-ray diffraction were obtained from the diffusion of ether into a DMF/pyridine solution of **8**.

Data for 8 (R = $CH_2{}^t$Bu). ^{1}H NMR (400 MHz, DMF-d_7): δ 12.1 (br s, 2H, H_2O), 10.0 (br s, 2H, H_2O), 9.08 (s, 2H, imine), 8.97 (s, 2H, imine), 8.87 (s, 2H, imine), 7.67 (s, 2H, Ar), 7.58 (s, 4H, Ar), 6.86 (s, 2H, Ar), 6.60 (s, 4H, Ar), 3.89 (s, 12H, O*CH*$_2$), 1.85 (s, 6H, OAc), 1.14 (s, 54H, $C(CH_3)_3$). UV−vis (CH_2Cl_2) λ_{max} (ϵ) = 241 (4.0×10^5) 360 (4.2×10^5), 421 (8.4×10^5) nm (L mol^{-1} cm^{-1}). MALDI-TOF: m/z = 1604.4 [**8** − AcOH + Na]$^+$. IR (KBr) ν = 2957, 2907, 2869, 1608, 1507, 1450, 1386, 1325, 1261, 1220, 1179, 1112, 1045, 1017, 925, 842, 762, 669, 614 cm^{-1}. Anal. Calcd for **8**, $C_{76}H_{92}N_6O_{17}Zn_4$·2DMF: N, 6.33; C, 55.66; H, 6.04. Found: N, 6.40; C, 54.90; H, 5.92.

Synthesis of the Heptazinc Methacrylate Complex 9 (R = C_2H_5). Zinc methacrylate (171 mg, 0.73 mmol) was added to a stirring suspension of macrocycle **1a** (100 mg, 0.10 mmol) in 15 mL of EtOH and refluxed for 11 h. The reaction was then cooled to room temperature, and 160 mg of a bright orange powder was isolated by filtration. The crude product was recrystallized from DMF to give **9** as a red, microcrystalline solid. Yield: 50 mg (25 μmol, 25%). Low solubility prevented analysis by ^{13}C NMR spectroscopy.

(22) Khanamiryan, A. K.; Bhardwaj, N.; Leznoff, C. C. *J. Porphyrins Phthalocyanines* **2000**, *4*, 484−490.

Data for 9 (R = C_2H_5). ^{1}H NMR (400 MHz, DMF-d_7): δ 8.85 (s, 6H, imine), 7.57 (s, 6H, Ar), 6.95 (s, 6H, Ar), 5.84 (d, $^2J_{HH}$ = 2 Hz, 3H, C=CH_2), 5.70 (d, $^2J_{HH}$ = 2 Hz, 3H, C=CH_2), 5.22 (s, 3H, C=CH_2), 5.10 (s, 3H, C=CH_2), 4.32 (q, $^3J_{HH}$ = 7.2 Hz, 12H, OCH_2), 1.74 (s, 9H, CH_3 methacrylate), 1.64 (s, 9H, CH_3 methacrylate), 1.47 (t, $^3J_{HH}$ = 7.2, 18H, OCH$_2$CH_3). UV−vis (CH_2Cl_2) λ_{max} (ϵ) = 241 (4.9×10^5) 347 (4.4×10^5), 415 (8.9×10^5) nm (L mol^{-1} cm^{-1}). MALDI-TOF: m/z = 1955.6^{9+}, 1872.5 [**9**−methacrylate]$^+$, 1722.1 [**9**−(methacrylate)$_2$−Zn + H]$^+$, 1637.3 [**9**−(methacrylate)$_3$−Zn]$^+$. IR (KBr) ν = 2960, 2925, 2839, 1612, 1561, 1508, 1463, 1419, 1394, 1319, 1268, 1221, 1187, 1108, 1040, 940, 831, 753, 669, 616, 558 cm^{-1}. Anal. Calcd for **9**: $C_{96}H_{114}N_6O_{25}Zn_7$·2DMF: N, 5.33; C, 47.97; H, 4.41. Found: N, 5.49; C, 47.45; H, 4.49.

Tetrazinc Methacrylate Complex 10 (R = C_2H_5). A round-bottom flask was charged with 51 mg (0.05 mmol) of macrocycle **1a** and 49 mg (0.21 mmol) of zinc methacrylate. The mixture was cooled to 0 °C in an icebath, and 20 mL of cold ethanol was added. After stirring at 0 °C overnight, the precipitate from the cloudy dark red-orange solution was isolated by centrifugation. The powder was purified by a second centrifugation with fresh ethanol. Compound **10** was dried under vacuum and obtained as a deep red powder (62 mg, 0.044 mmol, yield = 80%). Single crystals were grown from dimethylsulfoxide (DMSO). Low symmetry and poor solubility prevented analysis by ^{13}C NMR spectroscopy.

Data for 10 (R = C_2H_5). ^{1}H NMR (300 MHz, DMF-d_7): δ 10.0 (br s, 2H, H_2O), 8.91 (s, 2H, imine), 8.83 (s, 2H, imine), 8.77 (s, 2H, imine), 7.60 (s, 2H, Ar), 7.57 (s, 2H, Ar), 7.51 (s, 2H, Ar), 6.67 (s, 2H, Ar), 6.52 (s, 4H, Ar), 5.91 (s, 2H, C=CH_2), 5.29 (s, 2H, C=CH_2), 4.31 (br s, 12H, OCH_2), 1.81 (s, 6H, CH_3 methacrylate), 1.47 (t, $^3J_{HH}$ = 7.8 Hz, 18H, CH_2CH_3). UV−vis (CH_2Cl_2) λ_{max} (ϵ) = 421 (1.3×10^5), 350 (5.2×10^4) nm (L mol^{-1} cm^{-1}). MALDI-TOF: m/z = 1459.1 [**10** + $(H_2O)_2$ + H]$^+$. IR (KBr): ν = 3433, 2978, 2929, 2899, 1607, 1553, 1505, 1450, 1419, 1390, 1365, 1326, 1264, 1211, 1183, 1106, 1040, 942, 903, 887, 847, 832, 753, 734 cm^{-1}. Anal. Calcd for **10**·3H_2O ($C_{62}H_{66}N_6O_{20}Zn_4$): C, 50.42; H, 4.50; N, 5.69. Found: C, 50.43; H, 4.58; N, 5.74.

Crystallographic Studies. Data was collected on a Bruker X8 APEX diffractometer using Mo Kα radiation. Experimental details are summarized in Table 1. Single crystals of **7d**, **8**, and **10** were grown from DMF, DMF/pyridine ether diffusion, and DMSO, respectively. The structures were solved by direct methods with either *SIR1997*[23] or *SIR2002*[24] and further refined with *SHELXL-97*.[25] Fifteen DMF molecules were modeled in the unit cell of **7d** from the difference map with eight geometric restraints placed on the DMF molecule at the special position. Complex **8** crystallized with five DMF molecules per asymmetric unit, one of which was too disordered to be resolved from the difference map. The electron density from the disordered DMF molecule was accounted for using the SQUEEZE function of the *PLATON*[26] software package. Additionally, two aqua ligands were found coordinated in structure **8**, but the protons were not modeled. Two DMSO molecules were modeled with complex **10** by difference maps; the remaining solvent could not be modeled due to disorder, so the electron density was accounted for using the SQUEEZE function of *PLATON*. For each structure, all non-hydrogen atoms attached to the macrocycle were refined anisotropically, whereas hydrogen atoms were added at geometrically expected positions and left isotropic.

Table 1. Crystallographic Parameters for Compounds **7d**, **8**, and **10**

	7d	**8**	**10**
empirical formula	$C_{106.5}H_{154.5}N_{13.5}O_{32.5}Zn_7$	$C_{82}H_{102}N_8O_{20}Zn_4$	$C_{66}H_{70}N_6O_{18}S_2Zn_4$
M (g mol^{-1})	2601.53	1781.20	1560.98
cryst syst	triclinic	triclinic	triclinic
space group	$P\bar{1}$ (No. 2)	$P\bar{1}$ (No. 2)	$P\bar{1}$ (No. 2)
a (Å)	16.1439(12)	14.9100(12)	13.0855(21)
b (Å)	19.9971(14)	20.1369(16)	17.6039(33)
c (Å)	20.2118(11)	21.2381(17)	21.7220(40)
α (deg)	108.279(3)	62.141(4)	70.3680(80)
β (deg)	93.599(2)	81.526(4)	81.4740(70)
γ (deg)	99.512(3)	84.554(4)	70.9570(80)
V (Å^3)	6064.6(7)	5573.5(8)	4450.8(21)
Z	2	2	2
T (K)	173(2)	173(1)	173(2)
ρ_{calc} (g/cm^3)	1.425	1.061	1.165
λ(Mo Kα) (mm^{-1})	0.71073	0.71073	0.71073
F(000)	2716	1860	1608
θ range (deg)	1.5−25.3	1.8−26.9	1.7−28.3
reflns collected	96 897	113 091	81 131
indep reflns	21 651	23 540	20 789
obsd reflns [$I > 2\sigma$]	14 596	12 780	8512
R_{int}	0.0530	0.0781	0.0981
params refined	1442	1017	878
R1	0.0518	0.0755	0.0642
wR2	0.1529	0.2166	0.1549
GOF	1.032	1.016	0.885

Results and Discussion

Macrocycle Synthesis. While investigating the incorporation of zinc into the macrocycles, we were frustrated by the difficulties in obtaining clear NMR and MS identification of multimetallic intermediates. Consequently, we have worked to obtain crystallographic evidence for the compounds, and this has required us to vary the substituents on the macrocycles to promote crystallization. New macrocycle **1d** was prepared with the notion that the *tert*-butyl groups on the neopentyl chains would assist crystallization of the large complexes.

Macrocycle **1d** was prepared in four steps from catechol by the route illustrated in Scheme 2. Compound **2** was prepared in 81% yield using a literature procedure.[22] We conducted this reaction under several different conditions (e.g., K_2CO_3/DMF; NaOH/EtOH) that are effective for the preparation of analogues with *n*-alkyl chains, but it was necessary to use hexamethylphosphoramide (HMPA) to achieve a decent yield. Compound **2** was readily nitrated, and the nitro groups were subsequently reduced to give compound **4** in good overall yield. Schiff base condensation of **4** and **5** in $CHCl_3$/MeCN afforded macrocycle **1d** in 84% yield. Macrocycle **1d** is soluble in DMF and DMSO and shows a ^{1}H NMR spectrum that is characteristic of average D_{3h} symmetry. Matrix-assisted laser desorption ionization time-of-flight (MALDI-TOF) mass spectrometry confirmed that the macrocycle was the [3 + 3] product and not a larger cycle.

Heptametallic Zinc Clusters. Previously, we reported the unexpected formation of heptanuclear zinc cluster complexes

(23) *SIR1997*: Altomare, A.; Burla, M. C.; Camalli, M.; Cascarano, G. L.; Giacovazzo, C.; Guagliardi, A.; Moliterni, A. G. G.; Polidori, G.; Spagna, R. *J. Appl. Crystallogr.* **1999**, *32*, 115−119.
(24) *SIR2002*: Burla, M. C.; Camalli, M.; Carrozzini, B.; Cascarano, G. L.; Giacovazzo, C.; Polidori, G.; Spagna, R. *J. Appl. Crystallogr.* **2003**, *36*, 1103.
(25) Sheldrick, G. M. *SHELXL-97*; University of Göttingen: Göttingen, Germany, 1997.
(26) Spek, A. L. *PLATON*; Utrecht University: Utrecht, The Netherlands, 2002.

Scheme 2. Preparation of Macrocycle **1d**

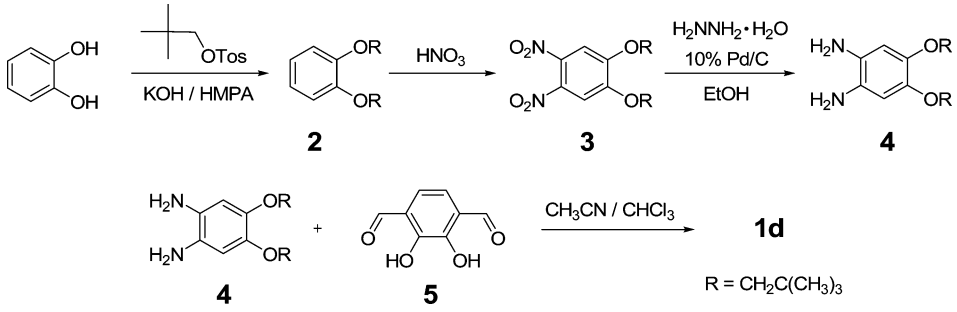

7a−**c** upon reacting macrocycles **1a**−**c** with an excess of zinc acetate. Single-crystal X-ray diffraction (SCXRD) studies of **7a** and **7b** revealed that the complexes consist of a trimetalated macrocycle with each N_2O_2 pocket coordinated to a zinc ion and a distorted tetrahedral $[Zn_4O]^{6+}$ cluster fastened to the macrocycle through bridging acetate ligands. We have since established by MALDI-TOF mass spectrometry, SCXRD, and NMR spectroscopy that reacting macrocycle **1d** with an excess of zinc acetate also yields a heptanuclear zinc cluster complex, **7d** (Figure 1). As expected, cluster complex **7d** is very similar to complexes **7a** and **7b**. The structural consistency supports the rigidity of the macrocycle-cluster complex and suggests that the peripheral alkyl chains, which aid in solubility, have little influence on the coordination environment found in the interior of the macrocycles.

Because of the high symmetry of heptazinc complexes **7a**−**d**, only one imine, two aromatic, and two acetate resonances are observed in their ^{1}H NMR spectra. The OCH_2 resonance of the neopentyloxy substituents is a singlet for macrocycle **1d**, but appears as two doublets for complex **7d**. This indicates that the two methylene protons in **7d** are diastereotopic and display geminal coupling of 8.8 Hz. Similarly, the OCH_2 resonances in **1a**−**c** are triplets, whereas **7a**−**c** all show complex coupling patterns that were simulated as an ABX_2 spin system. The protons on the OCH_2 for **7a**−**c** are inequivalent and display both geminal and vicinal coupling. Since macrocycles **1a**−**d** clearly exhibit C_3 rotational symmetry in solution and ^{13}C NMR spectroscopy indicates that there is only a single OCH_2 carbon environment, the horizontal plane of symmetry in the macrocycle must be absent from **7a**−**d**, leading to diastereotopic H atoms in the OCH_2 group. These spectroscopic observations support the structural assignment.

Peaks corresponding to the molecular ion or fragment ion $[M-OAc]^+$ are observed by MALDI-TOF mass spectrometry for each heptazinc complex, further confirming their structures. In the case of **7d**, peaks found by MALDI-TOF MS at *m*/*z* 1604.3, 1746.3, and 1811.3 are assigned to tetra-, penta-, and hexazinc fragments. Similar fragmentation patterns are observed for **7a**−**c** using soft ionization techniques.

Complexes **7a**−**d** are isolated as deep red to bright orange powders but all appear deep red upon dissolution in CH_2Cl_2, $CHCl_3$, DMSO, or DMF. The nearly superimposable electronic absorption spectra of the complexes are dominated by three peaks. Of the three, the highest intensity absorption is between 413 and 419 nm with a shoulder found between 346 and 348 nm. These peaks are most likely π or n to π^* transitions since similar absorptions are observed for macrocycles **1a**−**d** prior to metal coordination (406 and 343 nm for **1d**). The final absorption exhibits similar intensity to the shoulder and is located between 240 and 242 nm. Basic zinc acetate exhibits a ligand-to-metal charge transfer (LMCT) band at 216 nm, leading us to believe this final absorption

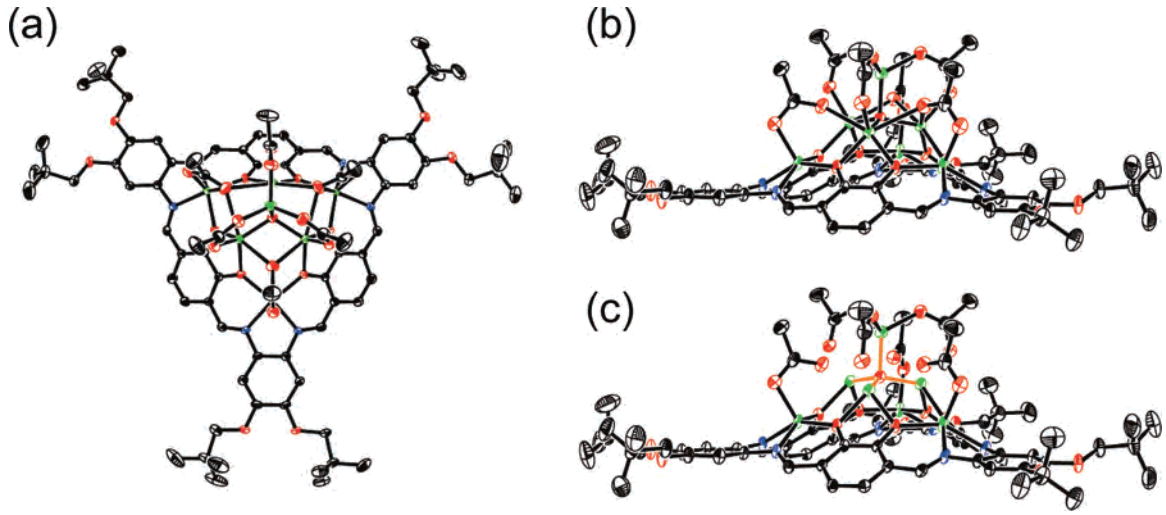

Figure 1. ORTEP depictions of heptazinc metallomacrocycle **7d** crystallized from DMF: (a) Top view of the complex. (b) Side view of the complex. (c) Side view of the complex with the Zn−O bonds of the central $[Zn_4O]^{6+}$ cluster highlighted in orange (some bonds have been removed for clarity). All ellipsoids are at 50% probability with hydrogen atoms omitted. (C = black, N = blue, O = red, Zn = green.)

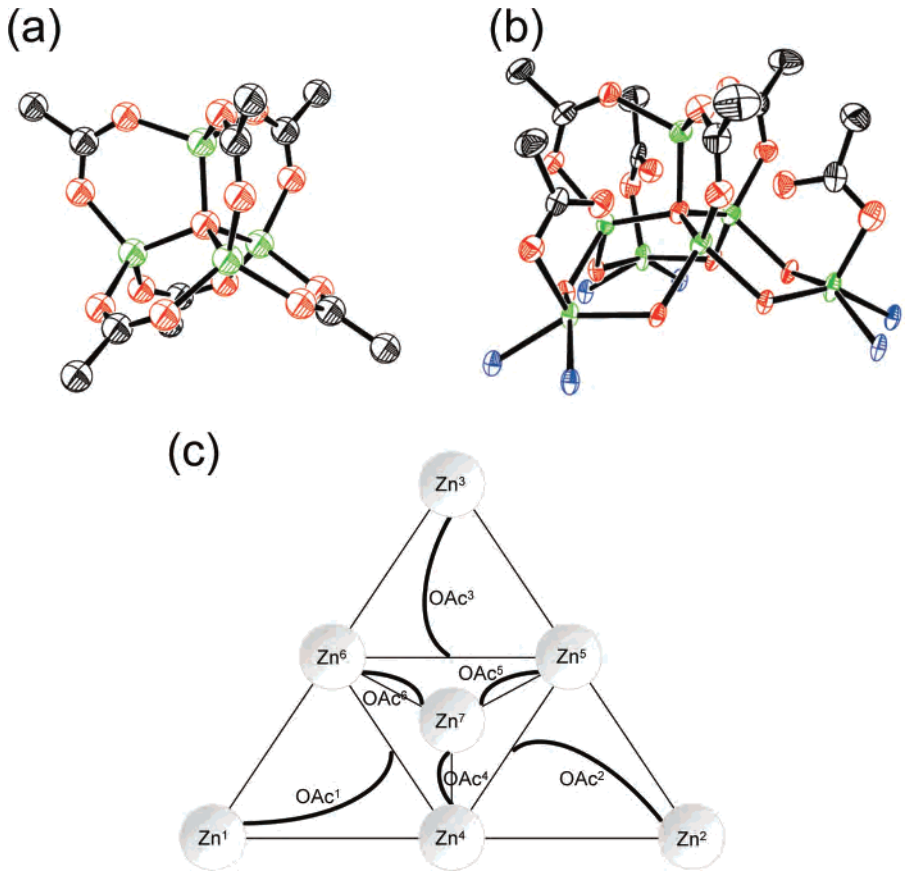

Figure 2. (a) Tetrahedral basic zinc acetate cluster, $[Zn_4O(OAc)_6]$. (b) Distorted tetrahedral $[Zn_4O]^{6+}$ cluster from complex **7d** (the macrocycle portion of **7d** has been omitted). Thermal ellipsoids are at 50% probability with hydrogen atoms removed for clarity. (C = black, N = blue, O = red, Zn = green.) (c) Schematic of the heptazinc cluster templated by macrocycles **1a**−**d** with individual zinc ions and acetate ligands labeled for bond length comparison.

is also a LMCT band,[27] though it may also be associated with the large conjugated macrocycle present in **7a**−**d**.

The near-tetrahedral $[Zn_4O]^{6+}$ acetate clusters within structures **7a**−**d** are very similar to basic zinc acetate. Figure 2 depicts basic zinc acetate and the $[Zn_4O]^{6+}$ acetate cluster portion of complex **7d**. For the purpose of comparing bond lengths, Figure 2c shows the arrangement of the metal ions and acetate ligands in complexes **7a**−**d**. Selected bond lengths of the capping cluster are summarized in Table 2. The Zn^{2+} ions are designated as Zn^1−Zn^7 and the acetate bridging ligands as OAc^1−OAc^6, as shown in Figure 2c. The three Zn^{2+} ions within the N_2O_2 pockets of the macrocycle are Zn^1, Zn^2, and Zn^3 (square pyramidal), those at the bottom of the tetrahedral capping cluster are Zn^4, Zn^5, and Zn^6 (distorted octahedral), while the lone Zn^{2+} ion at the top of the capping cluster is Zn^7 (tetrahedral). The acetate ligands that bridge the macrocycles to the capping clusters in a μ-1,1,2 fashion are designated OAc^1, OAc^2, and OAc^3 while those linking the bottom of the $[Zn_4O]^{6+}$ tetrahedron (Zn^{4-6}) to the top (Zn^7) are OAc^4, OAc^5, and OAc^6. Basic zinc acetate may be visualized as the tetrahedron made up of Zn^4, Zn^5, Zn^6, and Zn^7 with bridging μ-1,2 acetate ligands OAc^4, OAc^5, and OAc^6. The other three acetate ligands found within basic zinc acetate are comparable to the $O-Zn^{(1-3)}-O$ (catechol oxygens) units in **7a**−**d**.

The most striking feature of complexes **7a**−**d** and basic zinc acetate is that each zinc cluster is centered about a tetrahedral μ_4-O atom with similar Zn−O bond lengths (Zn−μ_4-O distance is 1.966 Å in basic zinc acetate and 1.975 Å (average, Zn^7−μ_4-O) and 1.918 Å (average of symmetry equivalent Zn^4, Zn^5, and Zn^6−μ_4-O bonds) in complexes **7a**, **7b**, and **7d**). The deviations from tetrahedral symmetry in the $[Zn_4O]^{6+}$ cluster found within **7a**, **7b**, and **7d** may be attributed to electronic effects. Greater Lewis acid character exhibited by Zn^4, Zn^5, and Zn^6 due to their proximity to Zn^1, Zn^2, and Zn^3 in N_2O_2 pockets may account for the reduced average bond length between Zn^4, Zn^5, and Zn^6 and the central μ_4-O atom. This enhanced bonding also limits the electron density available for the μ_4-O−Zn^7 bond, in agreement with the observed longer bond. Steric effects may also play a role in the elongation of the μ_4-O−Zn^7 bond.

Besides carboxylate ligands, tetrahedral $[Zn_4O]^{6+}$ clusters have reported with carbamato,[28] phosphato,[29] formamidinate,[30] and *N*-heterocyclic[31] ligands. Within this family of basic zinc acetate analogues, the Zn−(μ_4-O) distances range

(27) Kunkely, H.; Vogler, A. *J. Chem. Soc., Chem. Commun.* **1990**, 1204−1205.

(28) (a) Dell'Amico, D. B.; Calderazzo, F.; Labella, L.; Marchetti, F. *Inorg. Chim. Acta* **2003**, *350*, 661−664. (b) McCowan, C. S.; Groy, T. L.; Caudle, M. T. *Inorg. Chem.* **2002**, *41*, 1120−1127. (c) Belforte, A.; Calderazzo, F.; Englert, U.; Strähle, J. *Inorg. Chem.* **1991**, *30*, 3778−3781.

(29) Lugmair, C. G.; Tilley, T. D.; Rheingold, A. L. *Chem. Mater.* **1997**, *9*, 339−348.

(30) Cotton, F. A.; Daniels, L. M.; Falvello, L. R.; Matonic, J. H.; Murillo, C. A.; Wang, X.; Zhou, H. *Inorg. Chim. Acta* **1997**, *266*, 91−102.

Table 2. Bond Lengths Pertaining to the Zinc Acetate Cluster of Complexes **7a**, **7b**, **7d**, and Basic Zinc Acetate[a,b]

bond	**7a** (Å)	**7b** (Å)	**7d** (Å)	average of **7a**, **7b**, and **7d** (Å)	basic zinc acetate (Å)
Zn^1-OAc^1	1.987(4)	2.072(5)	2.008(4)	2.012	
Zn^2-OAc^2	1.995(4)	1.992(4)	2.009(4)		
Zn^3-OAc^3	2.056(4)	1.983(4)	2.009(4)		
Zn^4-OAc^1	2.507(4)	2.437(5)	2.449(4)	2.555	
Zn^4-OAc^2	2.572(4)	2.719(4)	2.618(4)		
Zn^5-OAc^2	2.592(4)	2.749(4)	2.506(4)		
Zn^5-OAc^3	2.462(4)	2.473(4)	2.594(4)		
Zn^6-OAc^3	2.400(4)	2.576(4)	2.595(4)		
Zn^6-OAc^1	2.667(4)	2.591(4)	2.476(3)		
Zn^4-OAc^4	1.978(4)	1.966(4)	1.983(3)	1.974	1.976
Zn^5-OAc^5	1.977(4)	1.968(4)	1.974(4)		
Zn^6-OAc^6	1.979(4)	1.964(5)	1.973(4)		
Zn^7-OAc^4	1.981(4)	1.951(4)	1.966(4)	1.971	1.976
Zn^7-OAc^5	1.979(4)	1.961(4)	1.972(4)		
Zn^7-OAc^6	1.976(4)	1.973(5)	1.984(4)		
$Zn^4-\mu_4$-O[c]	1.916(4)	1.919(4)	1.913(3)	1.918	1.966
$Zn^5-\mu_4$-O	1.926(4)	1.921(4)	1.894(3)		
$Zn^6-\mu_4$-O	1.932(4)	1.927(4)	1.913(3)		
$Zn^7-\mu_4$-O	1.981(3)	1.975(4)	1.969(3)	1.975	1.966
$Zn^1\cdots Zn^4$	3.512(5)	3.547	3.501	3.536	
$Zn^1\cdots Zn^6$	3.602(5)	3.478	3.509		
$Zn^2\cdots Zn^4$	3.553(5)	3.497	3.559		
$Zn^2\cdots Zn^5$	3.568(5)	3.602	3.490		
$Zn^3\cdots Zn^5$	3.559(5)	3.573	3.498		
$Zn^3\cdots Zn^6$	3.523(5)	3.540	3.536		
$Zn^4\cdots Zn^5$	3.305(5)	3.249	3.256	3.259	3.210
$Zn^5\cdots Zn^6$	3.233(5)	3.195	3.251		
$Zn^6\cdots Zn^4$	3.315(5)	3.326	3.200		
$Zn^4\cdots Zn^7$	2.969(5)	2.966(1)	3.043(1)	3.003	3.210
$Zn^5\cdots Zn^7$	3.004(5)	3.078(1)	2.978(1)		
$Zn^6\cdots Zn^7$	2.987(5)	3.040(1)	2.966(1)		

[a] Zinc nuclei and acetate ligand labels correspond to Figure 2c. [b] The table is sectioned into bonds that are equivalent by symmetry in complexes **7a**, **7b**, and **7d**. [c] μ_4-O is the central oxygen of the $[Zn_4O]^{6+}$ tetrahedron.

from 1.84 to 2.01 Å, a span within which complexes **7a**, **7b**, and **7d** comfortably lie. Unusual heptazinc clusters consisting of two $[Zn_4O]^{6+}$ units that share a single octahedral Zn^{2+} ion have also been reported and have slightly longer $Zn-(\mu_4\text{-O})$ distances.[20]

Mechanistic Insight. Formation of **7** from **1** begins with the trimetalation of the macrocycle in the N_2O_2 sites. There are two probable avenues for formation of the tetrahedral cluster above the plane of the macrocycle: (1) the trimetalated macrocycle coordinates to a preformed basic zinc acetate cluster in solution or (2) the cluster is *template*d inside the metallomacrocycle.[32] A templation mechanism is most plausible because basic zinc acetate is generally synthesized by heating zinc acetate under a vacuum, eliminating acetic anhydride, but complexes **7** may be synthesized at room temperature (or even lower) and atmospheric pressure. Figure 3 shows a simple schematic comparing these two routes, neglecting the acetate and oxo ligands.

To investigate the possibility of a supramolecular templating mechanism such as that depicted in Figure 3b, we first synthesized a trizinc metallomacrocycle, hoping it would act as a scaffold to monitor the formation of the $[Zn_4O]^{6+}$ acetate cluster within macrocycles **1a**−**d.** The reaction of **1c** with 3 equiv of $Zn(OAc)_2$ gave a product with a very broad ^{1}H NMR spectrum. The ESI mass spectrum of the product indicates that the trizinc metallomacrocycle, complex **6c**, forms but also shows many species that correspond to aggregates (e.g., $[\mathbf{6c}_2]^{2+}$, $[\mathbf{6c}_2 + Zn]^{2+}$, $[\mathbf{6c}_3]^{2+}$). These results suggest that the trizinc metallomacrocycle can be prepared but that it aggregates strongly in solution. We have observed strong aggregation of larger macrocycles complexed to zinc.[9e] The absence of larger metallomacrocycle complexes such as **7c** in the MS and ^{1}H NMR spectra of the products from the trizinc reactions and the absence of hydroxyl protons in the NMR spectra lead us to conclude that complexation within the N_2O_2 pockets occurs prior to any cluster formation. Our attempts to isolate and characterize the trizinc complex using macrocycles with other substituents were also fraught with difficulties.

When macrocycle **1d** was reacted with 4 equiv of $Zn(OAc)_2$, a new product, **8** (Chart 1), was observed. Notably, in the ^{1}H NMR spectrum of complex **8**, the deshielded hydroxyl resonances are absent, indicative of zinc coordination to the N_2O_2 pockets. The equivalent integration of one acetate resonance, numerous aromatic resonances, and three distinct imine resonances suggests that a mirror plane is the only symmetry element present in the compound. The experimental ^{1}H NMR spectrum and proposed structure for complex **8** are shown in Figure 4. Two broad resonances located around 12 and 10 ppm were assigned to aqua ligands after obtaining a SCXRD structure. The molecular ion of tetrazinc complex **8** was not detectable by MALDI-TOF mass spectrometry, but instead the spectrum was dominated by the $[\mathbf{8}-AcOH + Na]^+$ fragment.

To confirm the structure of complex **8**, we grew single crystals by diffusing ether into a DMF/pyridine solution and conducting a SCXRD analysis. The solid-state structure is depicted in Figure 5. With the use of the labeling scheme from Figure 2c, Zn^1, Zn^2, and Zn^3 are found within each N_2O_2 pocket. They adopt a square-pyramidal geometry, distorting the macrocycle from near planar to concave. The Zn−O and Zn−N bond lengths of the N_2O_2 pockets range from 1.95 to 2.01 Å and from 2.06 to 2.11 Å, respectively. Zn^1 and Zn^2 are equivalent by a mirror plane (σ_h), and each has an axially coordinated acetate ligand that bridges to Zn.[4] An aqua ligand was found bound at the axial position of Zn^3.

The final zinc ion, Zn^4, exhibits square-pyramidal geometry and is coordinated to the interior of the macrocycle. The coordination sphere of Zn^4 is filled by a catechol group, two acetate ligands bridging from Zn^1 and Zn^2, and an aqua ligand directed at the center of the macrocycle. Most intriguing, the aqua ligand is perfectly poised to become the central

(31) Zheng, S.-L.; Zhang, J.-P.; Chen, X.-M.; Huang, Z.-L.; Lin, Z.-Y.; Wong, W.-T. *Chem.−Eur. J.* **2003**, *9*, 3888−3896.

(32) There are of course other more elaborate possibilities, such as the formation of a much larger complex that subsequently fragments, but the two suggested seem the most probable.

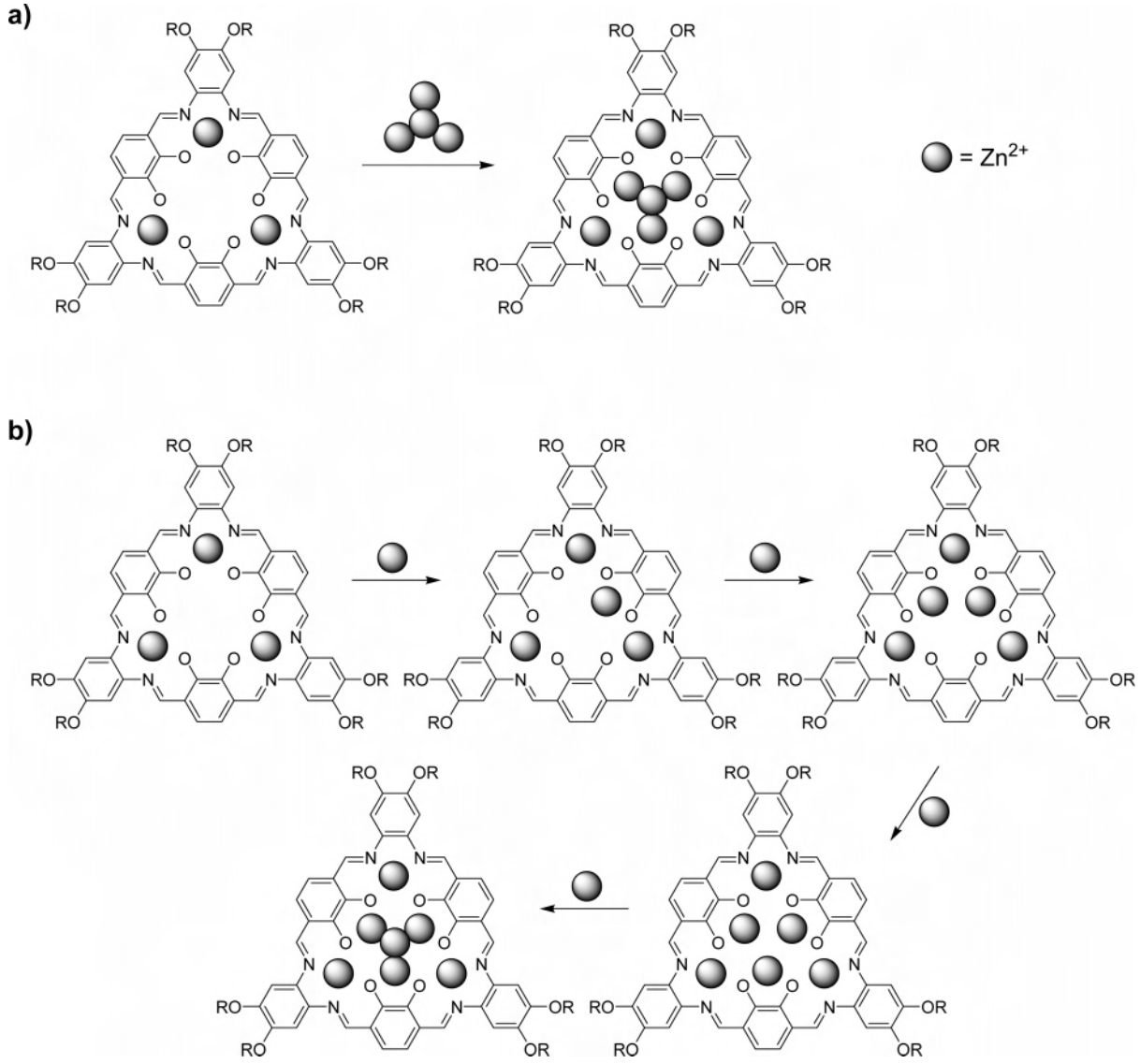

Figure 3. Two possible mechanisms for the formation of heptazinc complexes **7a**−**d**: (a) Basic zinc acetate forms in situ and coordinates to a trimetalated macrocycle or (b) the trimetalated macrocycle templates the cluster formation. Acetate ligands, coordinated solvent, and central μ_4-O atoms are omitted for clarity.

Chart 1. Structures of **8**−**10**

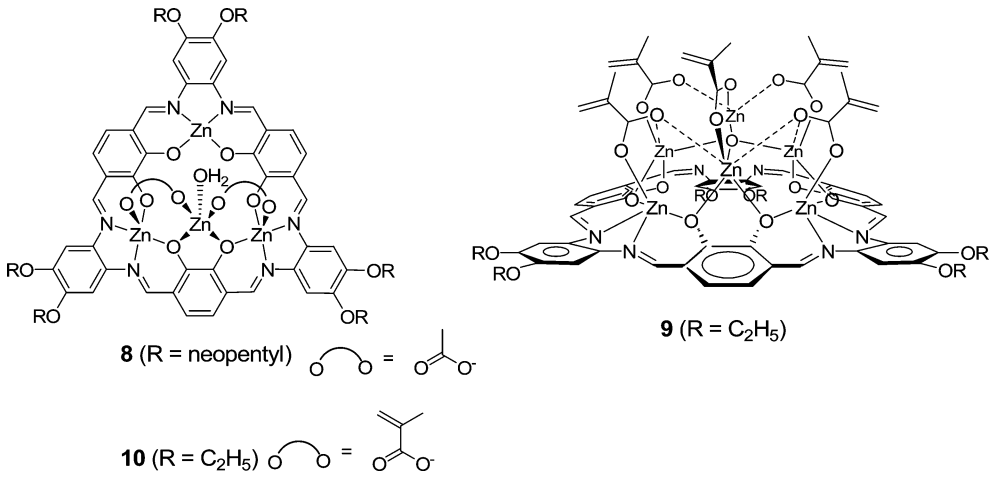

μ_4-oxo ligand of the $[Zn_4O]^{6+}$ acetate cluster found within complex **7d**. The Zn^4-O_{aqua} distance is 1.955 Å, very similar to the Zn−O distance in basic zinc acetate.

The templation of the tetrahedral zinc acetate cluster found in heptazinc metallomacrocycle **7d** begins with the coordination of Zn^4 above the plane of the trizinc macrocycle. To

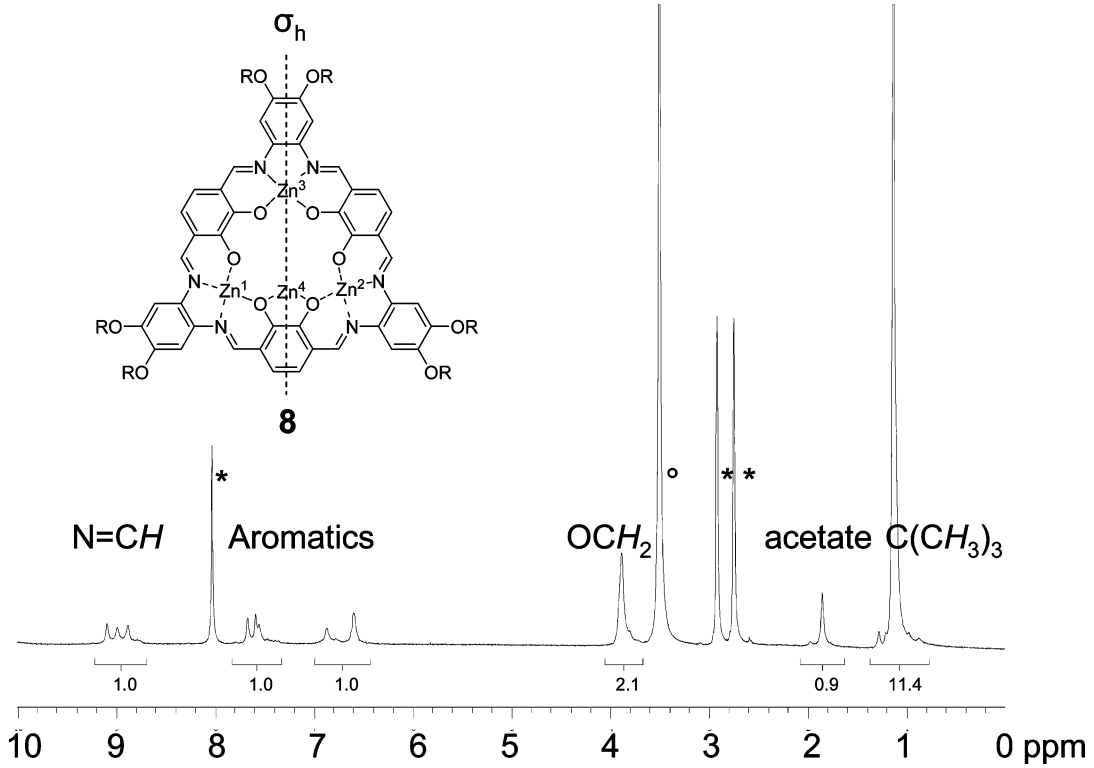

Figure 4. ^{1}H NMR spectrum of tetrazinc complex **8** in DMF-d_7 (400 MHz). The equivalent integration (6H) of three imine resonances, 5−6 aromatic resonances, and one acetate resonance is evidence for a single σ_h symmetry element and supports the inset structure (acetates have been omitted, and the zinc ions are labeled analagously to complexes **7a**−**d** in Figure 2c). DMF resonances are labeled with *, and nonbonded water is labeled with °. The magnetic environments about the OCH_2 and C(CH_3)$_3$ protons are only slightly perturbed by the broken symmetry and therefore appear as broad singlet resonances rather than as multiple peaks.

further understand this templating, we monitored the addition of $Zn(OAc)_2$ to complex **8** by ^{1}H NMR spectroscopy. The cluster growth was best observed in the aromatic and acetate regions shown in Figure 6. As $Zn(OAc)_2$ was incrementally added to a solution of **8**, new intermediate resonances arose but not in a smooth stepwise fashion. After exposure to 5.5 equiv of Zn^{2+} ions, the three imine and multiple aromatic resonances corresponding to complex **8** disappeared and resonances corresponding to the heptazinc complex **7d** became prominent. Upon further addition of zinc acetate, the single acetate resonance observed for complex **8** also disappeared and two resonances assigned to complex **7d** dominated the final spectrum.

Although the NMR titration presents evidence of other intermediates, possibly pentazinc or hexazinc complexes, during cluster templation, it was not possible to isolate these species. Crystals suitable for SCXRD could not be obtained from the addition of 5 or 6 equiv of $Zn(OAc)_2$ to any of macrocycles **1a**−**d**, and mass spectrometry provided little concrete evidence, as the heptametallic species is known to fragment to pentazinc and hexazinc species upon ionization.

Metal-Ion Ring Walking in Tetrazinc Complex 8 (R = $CH_2{}^tBu$). High-temperature ^{1}H NMR studies of complexes **7a**−**d** failed to show any intramolecular dynamic processes such as acetate exchange up to ∼120 °C; this is a testament to the robustness of the zinc complexes. We also used high-temperature ^{1}H NMR spectroscopy to probe fluxional behavior in complex **8**. When a sample of **8** in DMF-d_7 was heated, coalescence of the downfield resonances was observed, as shown in Figure 7. The spectral transformation is consistent with a change from C_s symmetry (observed in the SCXRD and room temperature ^{1}H NMR data) to three-fold symmetry. Specifically, the three imine resonances and six aromatic resonances coalesce to one and two resonances, respectively, resulting in a spectrum nearly identical to the C_3 symmetric heptazinc complexes **7a**−**d**. The process is reversible, and upon cooling back to room temperature, the original ^{1}H NMR spectrum of **8** showing C_s symmetry is obtained. This unexpected behavior implies that the fourth zinc ion, located within the central ring of the macrocycle, is labile, leading complex **8** to reversibly adopt a higher symmetry at elevated temperatures.

Kajiwara et al. observed similar behavior by variable-temperature NMR spectroscopy while studying a mononuclear Zn^{2+} complex of *p-tert*-butylsulfonylcalix[4]arene.[33] At room temperature, the aromatic protons of the calixarene are equivalent and exhibit a single resonance, suggesting that the zinc ion is walking between four equivalent tridentate sites. However, four different aromatic environments are observed in the ^{1}H NMR spectrum taken at −60 °C. At lower temperature, the Zn^{2+} ion is frozen in one environment on the NMR time scale but freely exchanges or "walks" between equivalent sites at higher temperature, as depicted in Figure 8a. Sekiguchi et al. also observed metal-ion ring walking by multinuclear NMR in a lithium salt of a [4]radialene dianion.[34]

(33) Kajiwara, T.; Yokozawa, S.; Ito, T.; Iki, N.; Morohashi, N.; Miyano, S. *Angew. Chem., Int. Ed.* **2002**, *41*, 2076−2078.

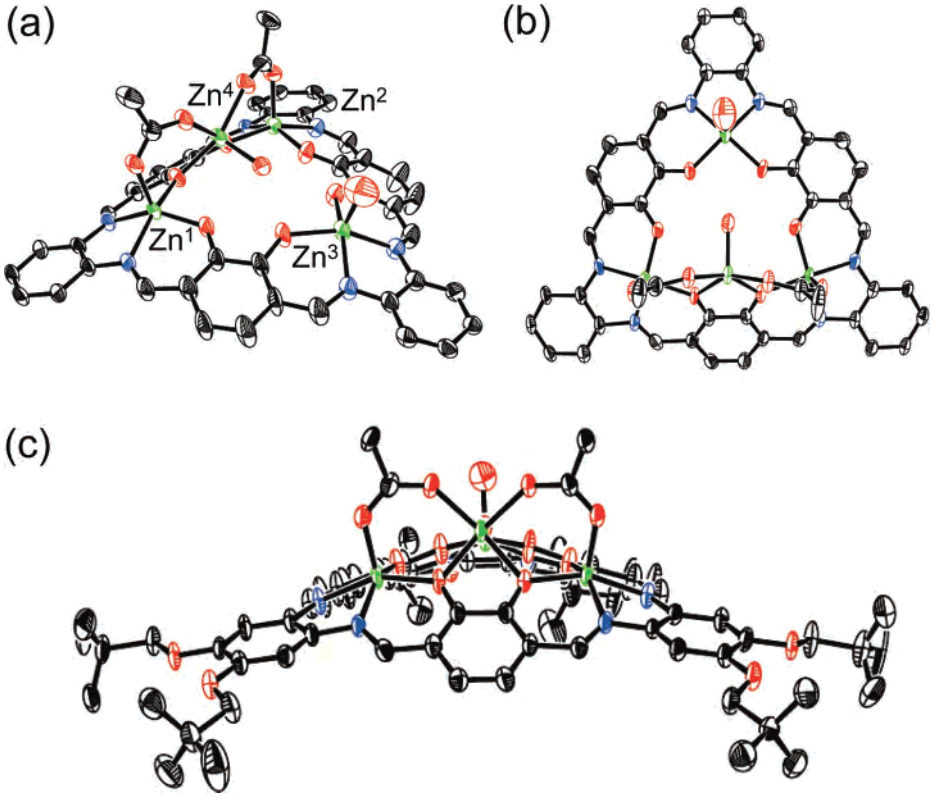

Figure 5. Solid-state structure of tetrazinc metallomacrocycle **8** as determined by SCXRD. (a) Side view of complex **8** revealing the central aqua ligand (the zinc ions have been labeled according to Figure 2c). (b) View from above; Zn^4 is projected out of the page. (c) Side view of Zn^4 bridged by acetates to Zn^1 and Zn^2. An aqua ligand completes the coordination sphere of Zn^3. Hydrogen atoms are omitted, and thermal ellipsoids are at 50% probability. Peripheral alkoxy chains have been omitted from a and b for clarity. (C = black, N = blue, O = red, Zn = green.)

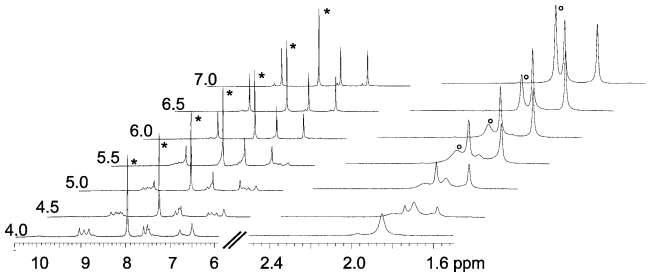

Figure 6. ^{1}H NMR spectra of the downfield and acetate regions during the stepwise addition of $Zn(OAc)_2$ in DMF-d_7 to a solution of tetrazinc complex **8**, resulting in the formation of heptazinc complex **7d**. The numbers on the left indicate the molar equivalents of zinc ions to macrocycle, * indicates DMF, and ° indicates free acetic acid that accumulates as complex **7d** forms.

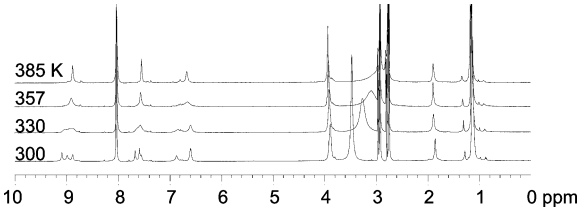

Figure 7. Variable-temperature ^{1}H NMR spectra of tetrazinc complex **8** in DMF-d_7 (400 MHz). As temperature is increased, the downfield imine and aromatic resonances coalesce, consistent with a shift from C_s to average 3-fold symmetry. This higher symmetry may be a result of the out-of-plane Zn^{2+} ion exchanging between three equivalent environments.

The coalescence observed in the ^{1}H NMR spectra of complex **8** upon heating can be explained by either Zn^{2+} ion ring walking as illustrated in Figure 8b or dissociation

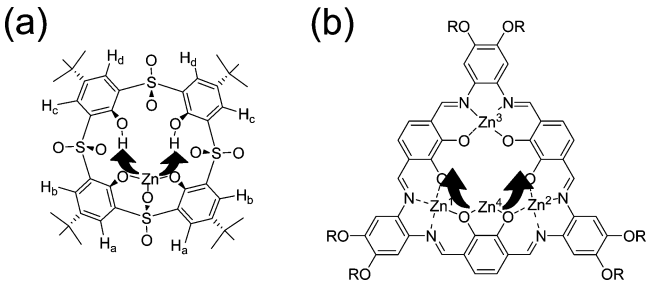

Figure 8. Illustration of Zn^{2+} ring walking in polydentate macrocycles. (a) Zn^{2+} exchanges between four equivalent sites in a sulfonylcalixarene.[34] (b) Proposed exchange of Zn^{2+} between three equivalent sites in tetrazinc complex **8**.

of the zinc ion and acetate ligands from the macrocycle. To test for dissociation, we added sodium acetate to a solution of **8** in DMF-d_7, heated the sample to 100 °C, and monitored the number of acetate resonances in the ^{1}H NMR spectrum. The presence of two different acetate resonances, one from free acetate and the other from complex **8**, would confirm Zn^{2+} ring walking whereas a single resonance would be evidence for dissociation (all the acetate is free in solution). Surprisingly, a reaction took place, and the ^{1}H NMR spectrum showed a mixture of products including heptazinc complex **7d** and other unidentifiable species, possibly the trizinc macrocycle (see the Supporting Information).

We attempted to isolate a trizinc complex **6d** of macrocycle **1d**, the hypothesized dissociation product of **8**, to

(34) Sekiguchi, A.; Matsuo, T.; Sakurai, H. *Angew. Chem., Int. Ed.* **1998**, *37*, 1661−1664.

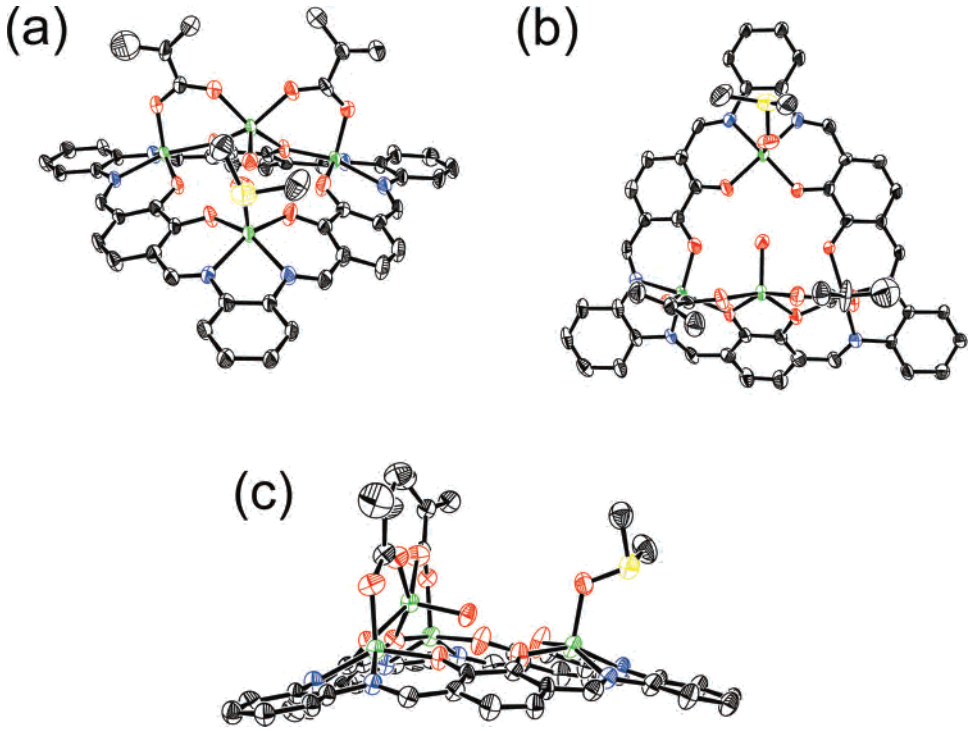

Figure 9. Solid-state molecular structure of complex **10** as obtained by SCXRD (hydrogen atoms and peripheral alkoxy groups are omitted for clarity). (a) View from the front. (b) Top down view. (c) Side view clearly showing the DMSO coordinated to Zn^3. Thermal ellipsoids are shown at 50% probability. (C = black, N = blue, O = red, Zn = green, S = yellow.)

compare the ^{1}H NMR chemical shifts in DMF-d_7 at 100 °C with those of complex **8** at 100 °C. Different chemical shifts would help confirm Zn^{2+} ring walking whereas identical shifts would be evidence for dissociation. Unfortunately, isolation of the trizinc complex of macrocycle **1d** was not possible. Elucidation of the dynamic behavior of **8** is still of interest to us.

Zinc Methacrylate Complexes. The investigation of zinc carboxylate cluster templation was expanded to include zinc methacrylate in an effort to alter the reactivity of the growing clusters, allowing for the study and isolation of possible intermediates. Reaction of macrocycle **1a** with an excess of zinc methacrylate afforded heptanuclear cluster complex **9** in 25% yield (Chart 1). The ^{1}H NMR spectrum of complex **9** showed one imine, two aromatic, and two CH_3 methacrylate resonances, identical to the analogous heptazinc complex **7a**. Four resonances were assigned to olefinic methacrylate protons, consistent with the existence of two carboxylate environments. Interestingly, the OCH_2 protons were chemical shift equivalent and appear as a quartet rather than an ABX_2 spin system as observed for the OCH_2 protons in complex **7a**. The molecular ion, [**9**]$^+$, and [**9**-methacrylate]$^+$ were both observed by MALDI-TOF mass spectrometry.

When 4 equiv of zinc methacrylate were reacted with macrocycle **1a**, a tetrazinc complex **10** was formed (Chart 1). The ^{1}H NMR spectrum of **10** is very similar to that of tetrazinc acetate complex **8**. Single crystals suitable for X-ray diffraction were obtained from DMSO, and the SCXRD analysis revealed a complex with four zinc centers, analogous to tetrazinc complex **8**. Each zinc ion exhibits square-pyramidal geometry, as depicted in Figure 9. Three Zn^{2+} ions occupy the N_2O_2 binding sites, imparting a saucer shape to the macrocycle, with Zn−O and Zn−N distances ranging from 1.96 to 2.05 Å and 2.10 to 2.16 Å, respectively. With the use of the labeling scheme from Figure 2c, methacrylate ligands are coordinated to the axial position of both Zn^1 and Zn^2. The axial position of Zn^3 is occupied by a DMSO molecule coordinated through a Zn−O interaction.

One zinc ion, Zn^4, is coordinated within the central ring of the macrocycle to the oxygen atoms of one catechol unit. Two methacrylate ligands bridging from Zn^1 and Zn^2 and an aqua ligand complete the coordination sphere of the capping Zn^4 ion. Much like complex **8**, the aqua ligand is centrally located and in perfect position to template the formation of **9**. The Zn^4-O_{aqua} distance is 1.966 Å, identical to the Zn−O distance in basic zinc acetate.

Tetranuclear complexes **8** and **10** represent trapped intermediates en route to heptanuclear cluster complexes **7d** and **9**, respectively. More studies will be required to fully elucidate what drives the templation of tetrahedral metal clusters inside macrocycles **1a**−**d**, but some conclusions may be drawn from the present work. Upon coordination of the N_2O_2 pockets, the zinc ions are forced into a pseudo-square-planar geometry due to the rigid nature of the conjugated macrocycles. Typically, four coordinate zinc ions prefer tetrahedral geometry, which is unachievable inside the N_2O_2 pockets, forcing them to adopt a square-pyramidal geometry by coordinating a carboxylate ligand in the apical position. This trizinc scaffold, with tethered carboxylate ligands, appears to be an optimal substrate to template clusters similar to basic zinc acetate.

Mixed-Metal Clusters from Tetrazinc Complex 8 (R = $CH_2{}^tBu$). Appealing candidates for the study of metalloenzyme mimics, mixed-metal clusters have been a long-

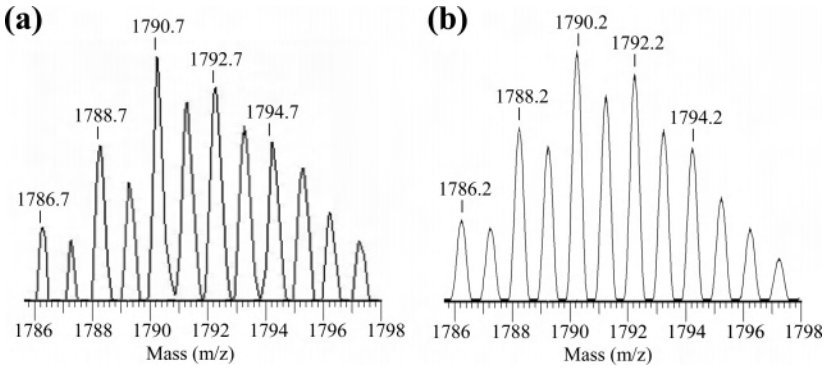

Figure 10. (a) MALDI-TOF isotopic distribution pattern of $[(\mathbf{1d}\text{-}6H)Zn_3Co_3O(OAc)_3]^+$. (b) Simulated isotopic distribution of the same ion.

standing target of synthetic inorganic chemists. Owing to the often unpredictable geometry and reactivity of metal clusters, the controlled synthesis of mixed-metal clusters poses a significant challenge. Complex **8** is an isolable, reactive intermediate with potential for further metal complexation. To demonstrate this potential, 4 equiv of cobalt(II) acetate were added to a suspension of **8** in EtOH and the mixture was heated to reflux. Cobalt(II) was chosen because it is known to form tetrahedral $[Co_4O]^{6+}$ clusters similar to basic zinc acetate.[35] A rusty orange, microcrystalline solid was isolated by filtration and subjected to a MALDI-TOF mass spectrometry study.

The mass spectrum revealed overlapping isotopic distributions centered about 1975.0 and 1968.6 amu that may be assigned to the mixed-metal clusters $[(\mathbf{1d}\text{-}6H)Zn_4Co_3O(OAc)_5]^+$ and $[(\mathbf{1d}\text{-}6H)Zn_3Co_4O(OAc)_5]^+$, respectively. Another peak corresponding to the cluster $[(\mathbf{1d}\text{-}6H)Zn_3Co_3O(OAc)_3]^+$ was resolved well enough for isotopic assignment, as displayed in Figure 10. This peak is likely due to a fragment of the previous two clusters, suggesting that the parent cluster is a mixed-metal complex that is structurally related to complex **7d**. This preliminary result illustrates the potential of complex **8** for generating mixed-metal clusters. Full characterization and crystallographic identification of these mixed-metal complexes is being pursued.

Conclusions

We have synthesized a new macrocycle with neopentyloxy substituents and have investigated the incorporation of zinc into Schiff base macrocycles **1a**−**d**. With an excess of zinc, a stable heptanuclear structure is obtained that may be described as a trizinc metallomacrocycle with a tetranuclear basic zinc acetate cluster in the macrocycle's interior. Crystallographic and NMR studies reveal that these complexes exhibit C_{3v} symmetry and have a closed bowl shape that is retained in solution. As a first step to elucidating the mechanism of zinc carboxylate cluster templation, two intermediates with four Zn^{2+} ions have been isolated and structurally characterized. We have also shown that heptanuclear complexes may be obtained by reacting the intermediate tetranuclear complexes with additional equivalents of zinc carboxylate. This provides evidence that a supramolecular templating mechanism may be active, with the macrocycle templating a molecular metal−oxo cluster in its interior.

This new system has potential for developing soluble cluster complexes that are applicable for catalysis or molecular magnets. We have demonstrated the ability to isolate reactive intermediates en route to larger metal clusters, a skill that has allowed for the synthesis of mixed ZnCo clusters and may aid in the development of polynuclear enzyme mimics. Expanding this chemistry to other metal ions and furthering our understanding of the mechanism of incorporation into these and related Schiff base macrocycles will continue to be the focus of our future research efforts.

Acknowledgment. We acknowledge the UBC and the Natural Sciences and Engineering Research Council (NSERC) of Canada for funding. A.J.G. and J.H.C. thank the NSERC for post-graduate fellowships. We also thank Marshall Lapawa for his help with mass spectrometry.

Supporting Information Available: Experimental details and supplementary spectra in PDF format and X-ray crystallographic data in CIF format for **7d**, **8**, and **10**. This material is available free of charge via the Internet at http://pubs.acs.org.

(35) Jaitner, P.; Rieker, C.; Wurst, K. *Chem. Commun.* **1997**, 1245−1246.

IC701385M